Macromolecules

ARTICLE

pubs.acs.org/Macromolecules

Cellular Crystallization in Thin Melt Film of it-Poly(butene-1): An Implication to Spherulitic Growth from Bulk Melt

Hiroshi Kajioka, Ken Taguchi, and Akihiko Toda*

Graduate School of Integrated Arts and Sciences, Hiroshima University, 1-7-1 Kagamiyama, Higashi-Hiroshima 739-8521, Japan

ABSTRACT: Crystallization of it-polybutene-1 (iPB-1) in form 2 from thin films of several tens of nanometers thick evolves a cellular structure composed of single-layered lamellar crystals. The dependences on thickness and crystallization temperature of the structure, namely of the cell width corresponding to the lamellar width, have been examined quantitatively. Temperature dependence of the cell width well agrees with the width of lamellar crystals grown from bulk melt, for the thin films with thickness in the same order in magnitude as the long spacing of crystal-melt stacks in the bulk melt. Crystallization from thin films is self-evidently controlled by mass transport under possible influence of compositions. The correspondence of the growth structures from thin films and from bulk melt therefore suggests the essential role of the gradient field of mass transport for lamellar branching in bulk melt, which eventually evolves polymer spherulites. The dependence of cell width on film thickness reflects the facility of mass transport in thicker melt films and the overgrowth on the single-layered lamellar crystals.

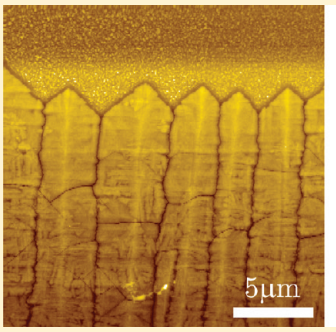

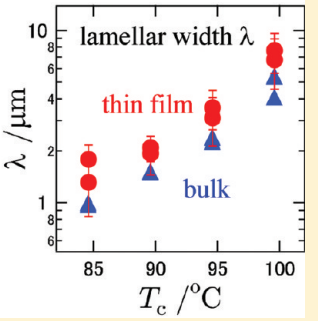

1. INTRODUCTION

With the developments of observation method by atomic force microscopy (AFM) and the growing interests in the properties of thin interface in nm-scale, there have been a number of reports on polymer crystallization from ultrathin films in recent years.[1−18] In general, crystallization of polymers proceeds as the growth of thin lamellar crystals of several to several tens of nanometers thick with chain folding.[19] Therefore, the growth from ultrathin films is one of the most suitable subjects to be examined. Various growth structures are evolved from thin films, such as dendrites, DLA (diffusion limited aggregation), labyrinthine patterns, etc.[1,2,5−13] Obviously, gradient field of mass transport (and possibly diffusion field of composition) in thin melt film plays a decisive role in the evolution of those structures.[9] In the present paper, we discuss the formation mechanism of a cellular structure, which evolves from thin films as an array of closely adjoined lamellae when started from preexisting seeds, as shown in Figure 1. The morphological evolution is examined in conjunction with the discussion on the structural formation of crystallization from bulk melt.

When crystallized from bulk melt, lamellar crystals get branched and reoriented (twisted) to fill in the three-dimensional space and eventually form a crystalline aggregate of so-called spherulite.[19] Spherulite is the basic structure of crystalline polymeric materials, and hence the formation mechanism has been one of the fundamental issues in polymer science and technology. In recent papers,[20−25] we have discussed the formation mechanism of spherulites and suggested the physical origin of lamellar branching as the growth front instability caused by a gradient field of chemical potential spontaneously formed in the melt ahead of the growth front. It has been suggested that mass transport (and/or composition) can be the origin of the gradient of chemical potential. The modeling and the predicted dependences on crystal growth rate, viscosity (diffusion coefficient), and molecular weight have been successfully confirmed for polyethylene (PE),[20,21] poly(vinylidene fluoride) (PVDF),[22] isotactic poly(butene-1) (iPB-1),[23,25] and isotactic polystyrene (iPS).[24] However, the direct confirmation of the existence of the gradient field in bulk melt has been a difficult issue, because of the inaccessibility to the growth front by direct observations. By utilizing the observation results on thin films, in which the existence of the gradient is self-evident, and comparing with those on spherulitic growth from bulk melt, we think we can convince ourselves of the role of gradient field in bulk melt, too.

Here, the mass transport is primarily required in order to compensate the crystal-melt density gap under the condition of steady state growth. For broad molecular weight and/or blended materials, molecular mobility determined by the compositions also plays an important role.[25] The mass transport is basically driven by pressure gradient, which induces melt flow toward the growth front. The gradient hence introduces negative pressure and the consequent melting point depression at the growth front. The variation of melting points corresponds to the gradient in the driving force of crystallization. Under the gradient in driving force, fluctuations of growth front can be accelerated, and eventually the growth front gets branched. This scenario is most

Received: August 30, 2011
Revised: October 18, 2011
Published: November 07, 2011

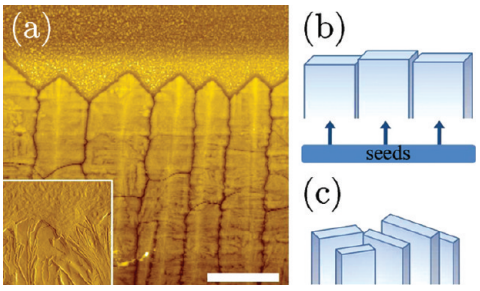

Figure 1. (a) AFM (height) image of the cellular growth of iPB-1 crystals grown from thin melt film (d = 60 nm) at 94.5 °C. The inset shows the growth front of spherulites grown from the bulk melt at the same temperature. The bar represents 5 μm. Schematic drawings of the growth from thin melt film and from the bulk melt are shown in parts b and c, respectively.

promoted for highly viscous polymer melt and evolves the spherulitic structure composed of finely branched lamellar crystals.

The critical lamellar width, λ, of branching is determined by both of the slope of the gradient in chemical potential, a, along the growth direction and the stabilizing surface tension, γ, as follows,[20]

$$\lambda = 2\pi\left(\frac{v_s\gamma}{a}\right)^{1/2} \quad (1)$$

where v_s represents the specific volume of a segment in the crystal. The gradient, a, is then represented by the pressure gradient along the growth direction, y, as $a = \Delta v(dp/dy)$ with the difference in the specific volume of a segment between the crystal and the melt, $\Delta v \equiv v_m - v_s$. When the mass transport is conducted by the shear flow of thickness, b, the flow rate, $\bar{u}$, is given as $\bar{u} = b^2(dp/dy)/(12\eta)$ with the gradient and the viscosity of polymer melt, η. The flow rate required to balance the density gap is given as

$$\bar{u} = V\Delta v/v_s \quad (2)$$

for the steady state growth with velocity, V. From those relationships, the critical lamellar width, λ, is represented as[20]

$$\lambda = 2\pi b\frac{v_s}{\Delta v}\left(\frac{\gamma}{12\eta V}\right)^{1/2} \propto (\eta V)^{-1/2} \quad (3)$$

and depends on the growth conditions which influence the viscosity, η, and the growth rate, V. We have successfully confirmed the relationship of eq 3 among λ, η, and V, experimentally.[20−25] The modeling of the gradient field of mass transport stems from original proposal by Keith and Padden[26,27] on the possible role of diffusion field of compositional gradient and from Schultz's suggestion[28] of possible negative pressure caused by the density gap at the growth front.

Under the gradient of composition and/or temperature, cellular pattern is a well-known dynamical structure of interface of crystal growth caused by an instability of Mullins−Sekerka type.[29−32] In the present case, the gradient should be primarily of mass transport in thin films with a possible influence of compositional gradient for broad molecular weight and/or blended materials. The uniqueness of the pattern is quite apparent, when compared with the growth front of spherulites from bulk melt (inset of Figure 1a), where the crystal-melt stacks form a mean periodic structure with the so-called long spacing in random

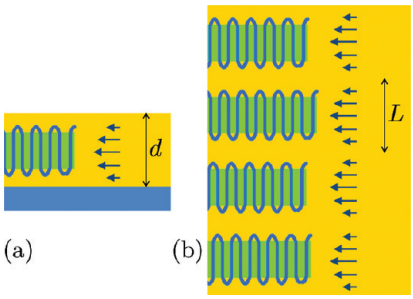

Figure 2. Cross-sectional views of the correspondence between (a) the growth from thin melt film of thickness, d, and (b) the growth from bulk melt with long spacing, L.

directions (Figure 2b). The pattern, i.e., the cell width, is determined by the destabilizing effect of the gradient and the stabilizing effect of surface tension in the same manner as the instability-driven branching reviewed in the above. Therefore, the expressions of the lamellar width, λ, in eqs 1 − 3 also apply to the cell width of the pattern. Here, in terms of the lamellar crystals in the bulk melt divided into a mean periodic structure of long spacing, we think that the growth environment will be regarded as comparable with the growth of single-layered lamellar crystals in thin films whose thickness, d, is in the same order in magnitude as the long spacing, L (Figure 2). It means that there should be a correspondence between the lamellar width of bulk melt and the cell width of thin films.

In the present paper, we examine the growth of the cellular structure evolved from thin films, the thickness of which is comparable with the long spacing of the crystallization from bulk melt. We examine the mean cell width in the cellular structure in comparison with the lamellar width at the growth front in the bulk melt. We think that similar variation in the widths will strongly support the decisive role of the gradient field of mass transport in the bulk melt as well as in thin films. In the following, we first construct the morphology diagram of the cellular structure depending on the film thickness and crystallization temperature. Second, we examine the temperature dependence of cell width in the cellular structure and compare the dependence with the lamellar width of bulk melt crystallization. Third, the thickness dependence is examined in detail to see the variation in the thickness range from ultrathin films up to the thickness much larger than the long spacing.

2. EXPERIMENTAL SECTION

Isotactic poly(butene-1), iPB-1, (M_w = 674 000, M_w/M_n = 4.7) was kindly supplied by Sun Allomer Ltd. For thin film preparation, a p-xylene solution of iPB-1 was prepared and spin-coated on a glass coverslip at 1000 rpm. The sample was then kept in a vacuum oven set at 80 or 130 °C for 3 h to vaporize the solvent; there was no noticeable influence of the drying temperature. The thickness of thin films was measured at a scratch by AFM, and was 20−500 nm for the solution concentration of 0.5−5.0 wt %, respectively.

Figure 3 shows the temperature protocol of melting, crystallization, and quenching by using a series of hot cells capable of temperature jumps.[33] The melting was conducted under vacuum. The quench was done by dropping the sample in freezing acetone, so that it was almost instantaneous. The recovering process from low temperature to room temperature after quenching was necessary in order to fix the quenched amorphous portions to be with the finest structure without the formation of large crystallites during the process above the glass transition temperature. Even with this careful procedure, the quenched portions

dx.doi.org/10.1021/ma201985h |Macromolecules 2011, 44, 9239–9246

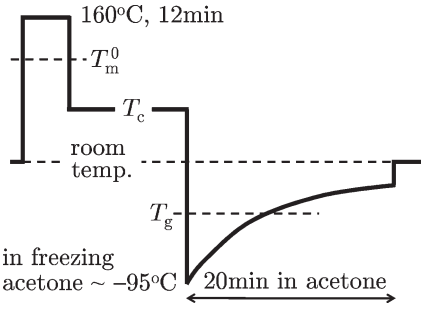

Figure 3. Temperature protocol of crystallization utilized in the present experiments: T_m^0 equilibrium melting temperature and T_g glass transition temperature.

were filled with small crystallites creating small protrusions, as recognized in Figure 1a. In Figure 1a and others, it is also noted that there are cracks and quasi-periodic small slits along normal to the growth direction in the lamellar crystals. Those are probably formed by volume change on quenching as well as on the solid−solid phase transition[34−36] from the original tetragonal Form 2[37,38] to the trigonal form 1[39] proceeded at room temperature. For the crystallization at high temperatures, in order to prepare seeds of crystalline aggregates forming the cellular structure, the edge of the glass coverslip was set outside the hot cell for melting. For low temperature crystallization, a large number of nuclei were spontaneously created, and the growth front became cellular.

The preparation method described above is essentially the same as that utilized in our previous works[23,25] on the crystallization of iPB-1 in form 2 from bulk melt, except for the seeding which was not necessary. For the quantitative comparison of the results of thin films of the present work and those of our previous work on bulk melt, the crystallization temperature, i.e., the degree of supercooling, was adjusted by the growth rate of spherulites from thick bulk melt. The absolute temperature in the hot cells was calibrated by a thermocouple embedded in a polymer film on a coverslip; the crystallization temperature for bulk melt in ref 23 is accordingly shifted by −2 °C in the present paper.

The morphology of the cellular structure in thin films was easily observed by AFM (SPI3800N, Seiko Instruments Inc.) and by phase contrast optical microscopy (phase-contrast OM, BX51, Olympus Corp.) without any pretreatments. In order to measure the height profile of crystals and to see the detailed structures, the quenched amorphous portions were removed by dropping the thin film in *p*-xylene instead of freezing acetone and by subsequent chemical etching of the method developed by Olley et al.,[40] as described in our prior paper.[23]

3. RESULTS AND DISCUSSION

Figure 4 shows typical growth morphology of iPB-1 crystals in the tetragonal form 2 grown from thin films. The preferred direction is [110] and the lateral habit at the growth front is basically squared with the {100} faces. On the three-dimensional shape of each lamellar crystal, it is also noted that they may not be completely planar, as indicated by the bright ridges along the growing [110] direction at the center of each cell. The nonplanarity of iPB-1 single crystals grown from dilute solution has been inferred from the curved edges of single crystals[34] reminiscent of bowl-like poly(4-methyl pentene-1) solution growth crystals.[41] The main cause of the nonplanarity will most probably be the surface stresses due to steric hindrance of chain folding, as has been extensively discussed by Lotz and Cheng.[42] The relevance to the formation of branches[43] should be addressed as well as of lamellar twist.[42] However, judged from the present AFM height images (the slope angle at the ridges <2°) and from

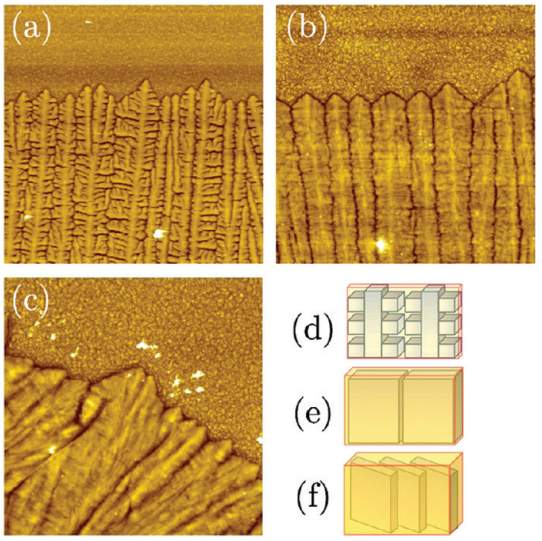

Figure 4. (a−c) AFM (height) images of the growth front of iPB-1 crystals grown from thin melt film (d = (a) 21, (b) 66, and (c) 136 nm) at 91.0 °C. The growth is (a) dendritic, (b) flat-on and individual, and (c) dis-oriented and multilayered, as schematically drawn in parts d−f, respectively. The image size is 20 × 20 μm^2.

reported dark-field images of the flat-on single crystals taken by transmission electron microscopy,[35,36] the titling angle of chains should be quite small compared with that of nonplanar PE crystals (tilt angle ~30°), so that the lamellar crystals could keep the growth to form the cell structure in thin films.

In comparison with the film thickness of d = 21−136 nm in Figure 4, it has been reported that the long spacing of the stacks of iPB-1 crystalline lamellae and amorphous layers is 30−40 nm thick in the temperature range examined.[44] On the other hand, for the molecular weight of the present sample, $M_w \simeq 7 \times 10^5$ g/mol, the radius of gyration of polymers is estimated to be $R_g \sim 40$ nm.[45] Figure 4a (d = 21 nm) shows the growth from ultrathin films thinner than the long spacing and R_g. Each cell is finely branched to be dendritic (Figure 4d). Recent extensive research of crystallization from ultrathin films is on the dendritic structures and the derivative of them. At thicker range but still in the same order in magnitude as the long spacing, the cells in Figure 4b (d = 66 nm) are composed of independent single-layered lamellar crystals, as schematically shown in Figure 4e. The growth from films much thicker than the long spacing is shown in Figure 4c (d = 136 nm). Cellular structure disappears, and lamellae are reoriented in three dimensions and stacked with each other to form multilayered structure corresponding to the growth from bulk melt (Figure 4f).

Figure 5 shows the morphology diagram plotted against film thickness, d, and crystallization temperature, T_c. In the examination of the T_c dependence of the cell width, the film thickness in the hatched area was chosen. In this thickness range, cellular structure of single-layered lamellar crystals is maintained without the appearance of dendritic structure or multilayering. It is noted that the thickness is thicker than the long spacing but remains in the same order in magnitude. The growth structures are of steady state growth with creation of cells by branching and with annihilation by collisions, as indicated in Figure 6; they are not the static structure simply formed as a consequence of geometric selection of growth directions among crystallites from seeds.

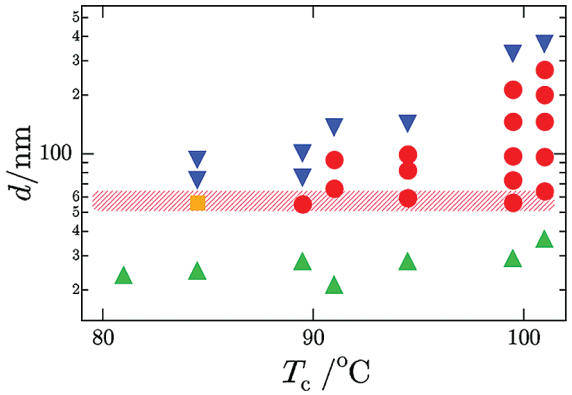

Figure 5. Morphology diagram in the thickness, d, vs crystallization temperature, T_c, plots. The symbols represent flat-on and individual (red ●), dendritic (green ▲), dis-oriented and multilayered (blue ▼), and intermediate growth (orange ■). The film thickness in the hatched area was chosen in Figures 6−9 for the comparison of cell width with the width of lamellae grown from the bulk melt.

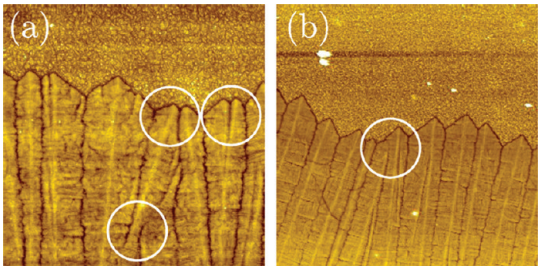

Figure 6. AFM (height) images of the growth front of iPB-1 crystals grown from thin melt film (d = 60−70 nm) at (a) 91.0 and (b) 96.0 °C. The circles indicate the events of creation and annihilation of lamellar branches. The image size is (a) 20 × 20 and (b) 50 × 50 μm^2.

AFM and phase-contrast OM images of Figures 7 and 8 show the T_c dependence of the cell structure. It is clearly seen that the cell width, i.e., lamellar width, became wider with increasing T_c, i.e. decreasing the growth rate, V. Figure 9 shows the plots of the cell width, λ, for the comparison with the lamellar width at the growth front of spherulites grown from bulk melt reported in ref.[23] Figure 9a shows the good agreement of the T_c dependence of λ for the growth from thin films and from bulk melt. Figure 9b shows the plots against ηV, according to the theoretical prediction of eq 3 with the temperature dependence of viscosity given as[46]

$$\eta_T = \exp\left[\frac{U/R}{T-(T_g-T_K)}\right] \quad (4)$$

where $T_g \simeq -24$ °C[47] represents the glass transition temperature, R is the gas constant, and the constants, U and T_K, are set at U = 4120 cal/mol and T_K = 51.6 K as "universal" constants.[46]

In Figure 9b, the fitting with the straight line of slope −0.5 is satisfactory, and suggests that the growth from thin film and from bulk melt satisfies the condition of the modeling. The agreement means that the determining process is the instability driven branching caused by similar type of gradient field for the growth from thin film and from bulk melt. If the growth pattern from thin films is driven by the gradient field of mass transport, so does the growth from bulk melt. For broad molecular weight and/or

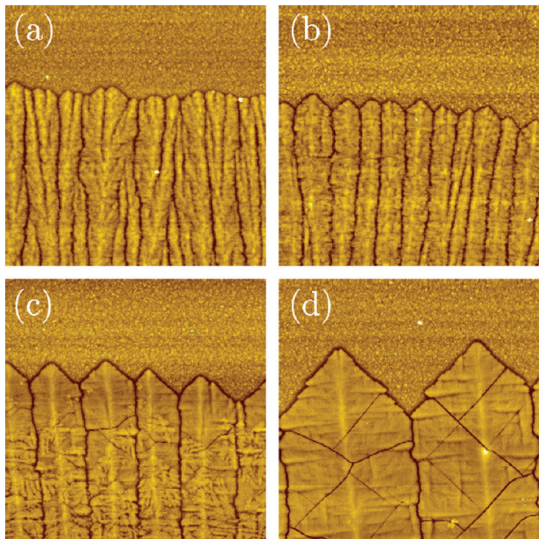

Figure 7. AFM (height) images of the growth front of iPB-1 crystals grown from thin melt film (d = 55−60 nm) at (a) 84.5, (b) 89.5, (c) 94.5, and (d) 99.5 °C. The image size is 20 × 20 μm^2.

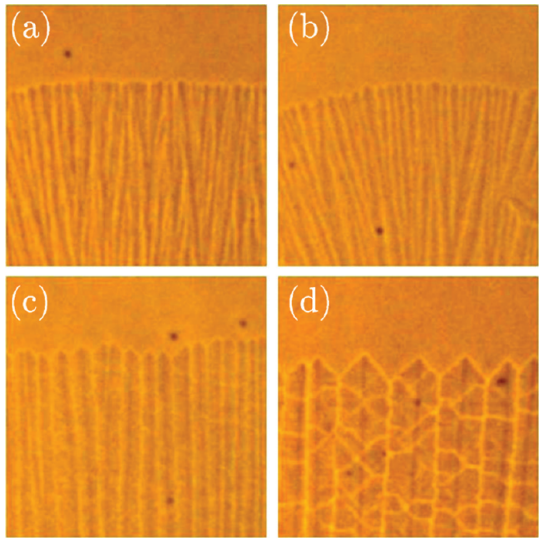

Figure 8. Phase-contrast OM images of the growth front of iPB-1 crystals grown from thin melt film (d = 55−60 nm) at (a) 84.5, (b) 89.5, (c) 94.5, and (d) 99.5 °C. The image size is 50 × 50 μm^2.

blended materials, it is also possible that the compositional gradient plays an important role both in thin film and bulk melt.

It is noted that the well-known thickness dependence of growth rate, V,[4] as shown in Figure 10, brought the relative shift of the data of thin films along the x-axis in Figure 9b of the plots against ηV and consequently the better agreement of the results of thin film and bulk melt in comparison with the plots in Figure 9a. For the present sample of iPB-1, the d dependence became appreciable for d < 80 nm. In the examined range of d = 55−60 nm, V becomes slower by about 70% of that for bulk melt. In addition, as a possible influence of film thickness, we can also think of the shift of glass transition temperature, T_g,[48−51] and the consequent effect on the viscosity, η, in the plots of Figure 9b. The effect is supposed to be appreciable for the system size in comparable

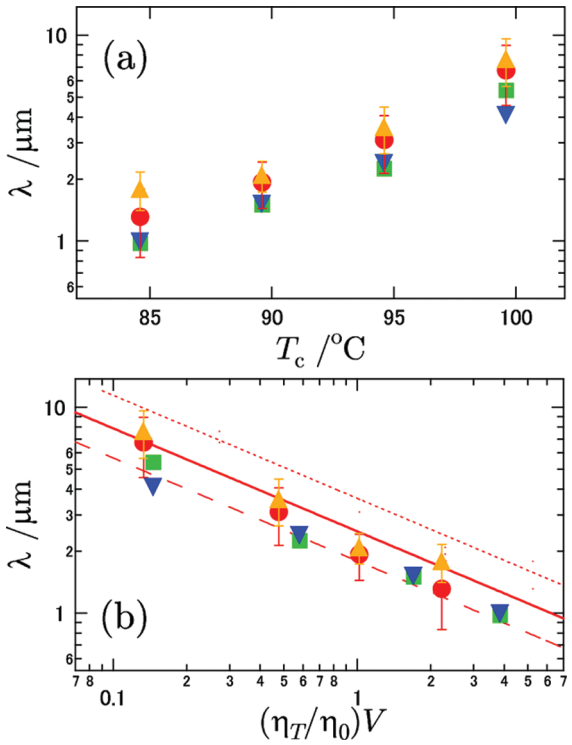

Figure 9. Plots of the cell (lamellar) width, λ, against T_c in (a) and against $(\eta_T/\eta_0)V$ in (b). The symbols represent the results of thin film AFM (red ●), thin film OM (orange ▲), bulk AFM (green ■), and bulk TEM (blue ▼). The film thickness was 55−60 nm. The slope of the straight lines in (b) is −0.5. The thick line represents the fitting to the results of thin films (red ●, orange ▲) with the x-axis of η_T common to both of thin film and bulk melt. The broken (dotted) line represents that for η_T with T_g of thin film 10 K lower (higher) than that of the bulk melt.

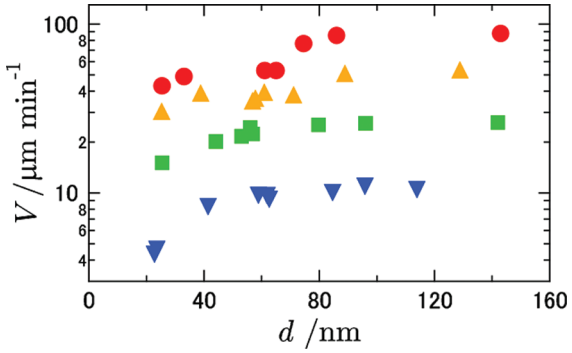

Figure 10. Plots of the growth rate, $V(T_c,d)$, against the film thickness, d, for T_c = 84.5 (red ●), 89.5 (orange ▲), 94.5 (green ■), and 99.5 °C (blue ▼).

with the radius of gyration of polymers, R_g. For the present sample, the radius of R_g ~40 nm is not negligibly smaller than the film thickness examined, d = 55−60 nm. Though the shift in T_g of iPB-1 has not been reported, the literature data of other polymers[49−51] may suggest the shift at most by several degrees. For reference purposes, the broken line in Figure 9b shows the fitting result with T_g of thin films 10 °C lower than that of bulk, and the dotted line for T_g 10 °C higher. Though it is not known whether T_g of iPB-1 on glass substrate becomes higher or lower,

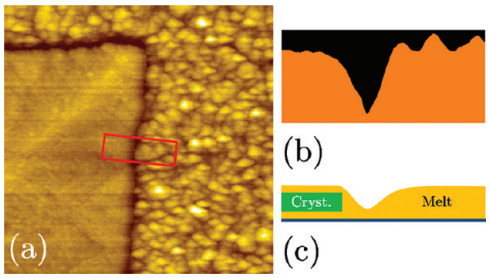

Figure 11. (a) AFM (height) image of the growth front of iPB-1 crystals grown from thin melt film (d = 64 nm) at 101.0 °C. The profile of surface height in the rectangular region is shown in (b), which has a thinner depletion zone along the growth front, as schematically shown in (c). The image size of part a is 5 × 5 μm^2, and the full scale of part b is height= 34 nm and width= 1.3 μm.

the literature data of other polymers[49−51] suggest the majority of the cases of lowering T_g with decreasing the size. As seen in Figure 9b, the case of lowering T_g brings better agreement of the results of thin film and of bulk melt. Those peculiar behaviors of crystal growth rate and glass transition in thin films have been ascribed to the effects of interfaces with substrate and air. Because our purpose is to prepare thin films having the corresponding environments to the growth of lamellar crystals in the crystal-melt stacks of bulk melt, we needed to avoid those influences specific to the interfaces, as possible as we could. For that purpose, we have chosen the film thickness, d = 55−60 nm, which is thicker than the radius of gyration of polymer, R_g ~ 40 nm, as well as than the long spacing, L = 30−40 nm, i.e. thick enough to have minimum effect of the depression in V and the shift of T_g.

For thin film growth, as a direct evidence of the gradient field of mass transport, there is depletion zone in the melt ahead of the crystal growth front.[3] Figure 11 clearly shows the existence in the present system. The width of the zone was less than 1 μm. Larger scale depletion zone, as seen in the crystallization of iPS from thin films,[3] was not recognizable in Figure 11 or other AFM images shown above, probably because of the obstacles of small protrusions of crystallites formed on the recovering process from quench to room temperature. Anyway, it is understandable that the direct confirmation of the gradient field was quite difficult for the growth from bulk melt.

Now, as the second part of the quantitative examination, Figure 12 shows the change in cellular structure with thickness, d, at two different T_cs. Parts a and b of Figure 12 show the change at relatively low crystallization temperature. The narrow lamellae did not show appreciable change in width. The cellular structure of single lamellar crystals shifts to the multilayered structure with increasing d. Parts c−f of Figure 12 show the results at higher temperature. Keeping the cellular structure in Figure 12, parts c and d, the cell became wider with increasing d, and reaches a maximum. Then, with further increasing d, the narrower cells in Figure 12e shift to the multilayered structure in Figure 12f having the lamellar width returning to those in the thin film of Figure 12c.

Figure 13 shows the d dependence of cell width, λ, determined at several different T_cs. The characteristic changes seen in Figure 12 are clearly recognized in the plots quantitatively. When combined with the morphology diagram of Figure 3, it is seen that the cell width of thinner film agrees well with the width of multilayered lamellae in thick film. The correspondence confirms similar environments for each lamellar crystal in multilayered

dx.doi.org/10.1021/ma201985h |*Macromolecules* 2011, 44, 9239–9246

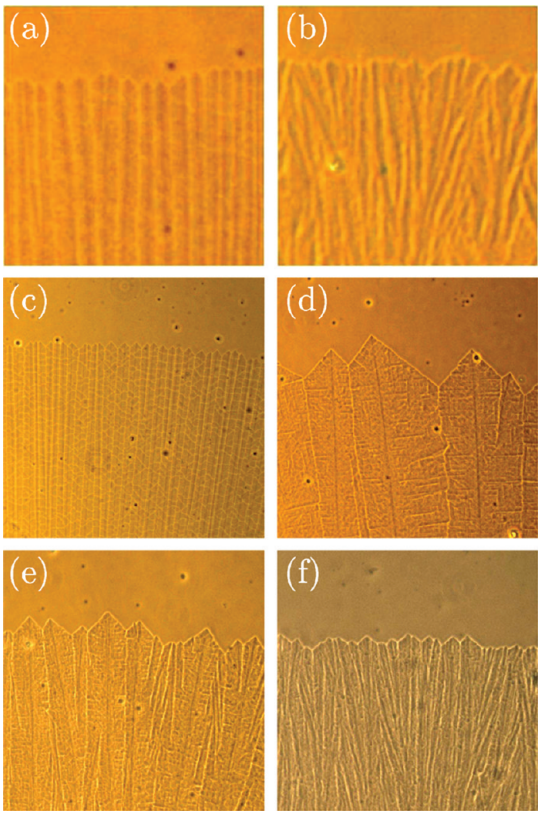

Figure 12. Phase-contrast OM images of the growth front of iPB-1 crystals grown from thin melt film at (a, b) 94.5 °C and (c–f) 99.5 °C: the film thickness, d = (a) 59, (b) 142, (c) 55, (d) 146, (e) 213, and (f) 275 nm. The image size is 50 × 50 μm^2 (a, b) and 200 × 200 μm^2 (c–f).

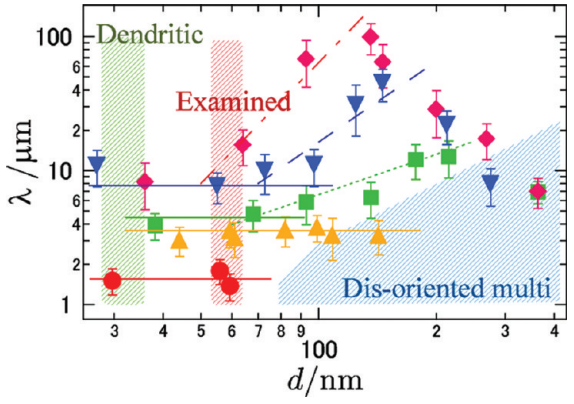

Figure 13. Plots of the cell width, λ, against film thickness, d. The symbols represent the results of T_c = 84.5 (red ●), 94.5 (orange ▲), 96.0 (green ■), 99.5 (blue ▼), and 101.0 °C (red ◆). The slopes of the dotted, broken, and alternating long and short dashed lines are 1, 2, and 3, respectively.

stacking of the bulk and in thin films, if the thickness of thin film is comparable with the long spacing of the multilayered stacking.

At lower T_c, probably due to narrower cell width, the multilayering with three-dimensional reorientation becomes easily dominant at thinner d, and, as a consequence, the width, λ, is kept unchanged with d. For the growth at higher T_c, much wider cells suppress the three-dimensional reorientation and multilayering

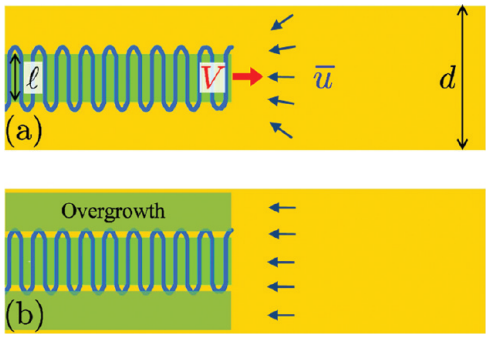

Figure 14. Schematic drawings of the growth in thin films: flat-on individual lamellar crystal (a) and the crystal with overgrowth (b).

and keep the cell structure even at much thicker d. Then, for the single-layered lamellar crystals in the cells, the mass transport should be much easier with films much thicker than the lamellar thickness, as schematically shown in Figure 14a. Easier mass transport means smaller gradient, and hence wider critical width, λ, for branching, as seen in eq 1. Namely, it is quite reasonable to have wider cell width with increasing d for the cells composed of single-layered lamellar crystals, as a consequence of smaller gradient field of mass transport. This variation in cell width with film thickness thus suggests additional confirming evidence for the determining effect of gradient field of mass transport.

For the lamellar crystal growing in the film, as shown in Figure 14a, the balance of mass transport across the growth front is represented as,

$$\frac{V}{\frac{\ell}{d}v_s + \frac{d-\ell}{d}v_m} = \frac{V+\bar{u}}{v_m} \tag{5}$$

where ℓ represents the crystalline thickness. For the case of $\ell = d$, eq 5 reduces to eq 2. Following the arguments in Introduction with the assignment of the thickness of shear flow equal to the film thickness, $b = d$ in eq 3, the shear flow of mass transport in the film predicts the following d dependence of critical λ

$$\lambda \propto d \text{ for } d = \ell \tag{6}$$

$$\propto d^{3/2} \text{ for } d \gg \ell \tag{7}$$

The predicted dependence suggests the power up to 1.5. Experimentally, the maximum power was about 3, as seen in Figure 13; the predicted dependence does not quantitatively account for the sharp rise in the cell width.

After reaching the maximum width, λ decreases with further increase in d, as seen in Figure 13 at high T_c. For this behavior, we noticed the influence of overgrowth on the fold surface, as schematically shown in Figure 14b and recognized in the AFM images of Figure 7. For the growth from 55–60 nm thick films in Figure 7, the fold surfaces were fully covered with overgrowth at lower T_c (Figure 7, parts a and b). With increasing T_c and decreasing the driving force of crystallization, the front of overgrowth retreated from the growth front of the main lamellae as seen in Figure 7c, and eventually disappeared from the view in Figure 7d. At the same T_c as of Figure 7d, the thickness dependence of overgrowth is shown in Figure 15. Parts a–c of Figure 15 show that, with increasing d, the overgrowth catches up the growth front even at high T_c. The AFM image of surface-

dx.doi.org/10.1021/ma201985h |*Macromolecules* 2011, 44, 9239–9246

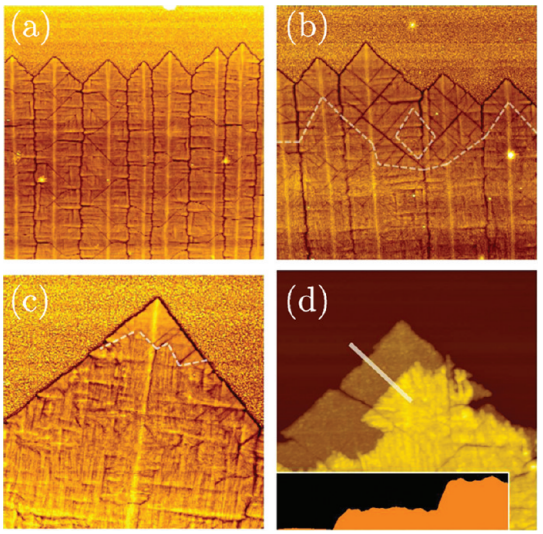

Figure 15. AFM (height) images of the growth front of iPB-1 crystals grown from thin melt film at 99.5 °C: the film thickness, d = (a) 55, (b) 98, (c) 147, and (d) 150 nm. The broken lines in parts b and c represent the fronts of overgrowth. The sample in part d was washed by xylene and chemically etched subsequently. The profile of surface height along the white bar in part d is shown in the inset (height = 160 nm and width = 6.6 μm). The image size is 50 × 49 μm^2 (a−c) and 20 × 20 μm^2 (d).

treated sample in Figure 15d suggests that the overgrowth is coherent with the main lamella in the crystallographic orientation. In addition, as clearly seen in Figures 7c and 15c, the overgrowth are formed by much smaller crystallites which nucleated on the surface of mother lamella. For those reasons, the overgrowth seems to be formed by long loops of chain folding and chain ends of the main lamellar crystal. The overgrowth therefore should be distinguished from multilayered stacks, in which lamellae are formed by branching and reorientation independently of each other.

In comparison with the single-layered lamellar crystal without overgrowth in Figure 14a, the overgrowth lined up with the growth front of the main lamella in Figure 14b will require the increase in mass transport and the consequent increase in the gradient field. In this way, at high T_c with further increase in d, the development of overgrowth will bring the decrease in λ, and eventually the structure shifts to the multilayered stacking of bulk melt.

In the final part of discussion, we may suggest a possible determination mechanism of long spacing in melt crystallization. In the scenario of the instability driven branching due to the gradient field of mass transport. we have been mainly concerned with the gradient along the growth direction. In terms of the thickness direction of lamellar stacks, there will be an interaction of the gradient field of mass transport of neighboring lamellae. Then, if the period of crystal-melt stacks is too short, the mass transport becomes less than necessary for keeping the steady state growth, and the lamellar crystal in thinner stack will be overcome by neighboring lamellae having enough supply of crystallizing molecules. On the other hand, if the spacing becomes too large, there will be a room to be filled by a new lamellar branch. In this way, the interaction of the gradient field of mass transport along the thickness direction can be the origin of optimum periodicity of crystal-melt stacks, which can be the long spacing, L. This speculation is based on the dependence of growth rate on melt thickness allocated to each lamellar crystal. The experimental examination will not be easy, because the thickness dependence of growth rate of flat-on lamellae in thin films can be caused by the effect of interfaces with the substrate and air, i.e., the effect on the mobility of chains near the interfaces, as well as simply by the effect of melt thickness on mass flow. We may approach this issue by examining the growth of edge-on lamellae in thin films or on the melt surface to see the effects of multilayering on the growth rate; actually, large fluctuations in growth rates of edge-on lamellae have been reported by in situ AFM observation of growth on the melt surface.[52]

4. CONCLUSIONS

We have examined the growth of cellular structure of iPB-1 on crystallization from thin films, the thickness of which is in the same order in magnitude as the long spacing, i.e. the period of crystal-melt stacks in bulk melt. The temperature dependence of cell (lamellar) width clearly suggested the correspondence between the growth from bulk melt, which is subdivided into the crystal-melt stacks in the thickness direction, and the growth from thin film, the thickness of which is comparable with the long spacing. The cell (lamellar) width under both conditions followed the temperature dependence predicted from the modeling of instability-driven branching of lamellar crystals set in a gradient field of chemical potential in the melt ahead of the growth front. The present result experimentally supports the decisive role of the gradient not only for the growth from thin films, for which the effect is self-evident, but also for bulk melt. The growth pattern from thin film is most probably driven by the gradient in mass transport with possible influence of compositions for broad molecular weight and/or blended materials. The result hence supports the suggestion of the spherulitic growth of polymer crystallization from bulk melt based on the modeling of instability-driven lamellar branching coupled with noncrystallographic reorientation due to excess stresses of folding surfaces.

AUTHOR INFORMATION

Corresponding Author

*Telephone: +81-82-424-6558. Fax: +81-82-424-0757. E-mail: atoda@hiroshima-u.ac.jp.

ACKNOWLEDGMENT

The authors wish to thank Prof. S. Tanaka of Hiroshima University and Prof. Y. Yamazaki of Waseda University for helpful discussions. This work was supported by KAKENHI (Grant-in-Aid for Scientific Research on Priority Area "Soft Matter Physics" from the Ministry of Education, Culture, Sports, Science and Technology of Japan.

REFERENCES

(1) Lovinger, A. J.; Cais, R. E. *Macromolecules* **1984**, *17*, 1939.
(2) Sakai, Y.; Imai, M.; Kaji, K.; Tsuji, M. *J. Cryst. Growth* **1999**, *203*, 244.
(3) Izumi, K.; Ping, G.; Toda, A.; Miyaji, H.; Hashimoto, M.; Miyamoto, Y.; Nakagawa, T. *Jpn. J. Appl. Phys.* **1994**, *33*, L1628.
(4) Sawamura, S.; Miyaji, H.; Izumi, K.; Sutton, S. I.; Miyamoto, Y. *J. Phys. Soc. Jpn.* **1998**, *67*, 3338.
(5) Taguchi, K.; Miyaji, H.; Izumi, K.; Hoshino, A.; Miyamoto, Y.; Kokawa, R. *Polymer* **2001**, *42*, 7443.

(6) Taguchi, K.; Toda, A.; Miyamoto, Y. *J. Macromol. Sci. Phys.* **2006**, *B45*, 1141.
(7) Reiter, G.; Sommer, J.-U. *Phys. Rev. Lett.* **1998**, *80*, 3771.
(8) Reiter, G.; Sommer, J.-U. *J. Chem. Phys.* **2000**, *112*, 4376.
(9) Grozeva, N.; Botizb, I.; Reiter, G. *Eur. Phys. J.* **2008**, *E27*, 63.
(10) Beers, K. L.; Douglas, J. F.; Amis, E. J.; Karim, A. *Langmuir* **2003**, *19*, 3935.
(11) Okerberg, B. C.; Marand, H.; Douglas, J. F. *Polymer* **2008**, *49*, 579.
(12) Zhai, X.; Wang, W.; Zhang, G.; He, B. *Macromolecules* **2006**, *39*, 324.
(13) Zhang, G.; Jin, L.; Zheng, P.; Shi, A.-C.; Wang, W. *Polymer* **2010**, *51*, 554.
(14) Mareau, V. H.; Prud'homme, R. E. *Macromolecules* **2005**, *38*, 398.
(15) Liu, Y.-X.; Chen, E.-Q. *Coord. Chem. Rev.* **2010**, *254*, 1011.
(16) Ramanathan, M.; Darling, S. B. *Prog. Polym. Sci.* **2011**, *36*, 793.
(17) Schoönherr, H.; Frank, C. W. *Macromolecules* **2003**, *36*, 1199.
(18) Zhu, D.-S.; Liu, Y.-X.; Chen, E.-Q.; Li, M.; Chen, G.; Sun, Y.-H.; Shi, A.-C.; Van Horn, R. M.; Cheng, S. Z. D. *Macromolecules* **2007**, *40*, 1570.
(19) Geil, P. H.; *Polymer Single Crystals*; John Wiley: New York; 1963.
(20) Toda, A.; Okamura, M.; Taguchi, K.; Hikosaka, M.; Kajioka, H. *Macromolecules* **2008**, *41*, 2484.
(21) Toda, A.; Taguchi, K.; Kajioka, H. *Macromolecules* **2008**, *41*, 7505.
(22) Toda, A.; Taguchi, K.; Hikosaka, M.; Kajioka, H. *Polym. J.* **2008**, *40*, 905.
(23) Kajioka, H.; Hikosaka, M.; Taguchi, K.; Toda, A. *Polymer* **2008**, *49*, 1685.
(24) Kajioka, H.; Yoshimoto, S.; Taguchi, K.; Toda, A. *Macromolecules* **2010**, *43*, 3837.
(25) Kajioka, H.; Yamada, K.; Taguchi, K.; Toda, A. *Polymer* **2011**, *52*, 2051.
(26) Keith, H. D.; Padden, F. J., Jr. *J. Appl. Phys.* **1963**, *34*, 2409.
(27) Keith, H. D. *J. Polym. Sci.* **1964**, *A2*, 4339.
(28) Schultz, J. M.; *Polymer Crystallization*; Oxford University Press: Oxford, U.K., 2001, Chapter 10.
(29) Mullins, W. W.; Sekerka, R. F. *J. Appl. Phys.* **1963**, *34*, 323.
(30) Mullins, W. W.; Sekerka, R. F. *J. Appl. Phys.* **1964**, *35*, 444.
(31) Langer, J. S. *Rev. Mod. Phys.* **1980**, *52*, 1.
(32) Tiller, W. A.; *The Science of Crystallization: Macroscopic Phenomena and Defect Generation*; Cambridge University Press: New York, 1991, Chapters 5 and 6.
(33) Toda, A.; Kojima, I.; Hikosaka, M. *Macromolecules* **2008**, *41*, 120.
(34) Holland, V. F.; Miller, R. L. *J. Appl. Phys.* **1964**, *35*, 3241.
(35) Kopp, S.; Wittmann, J. C.; Lotz, B. *J. Mater. Sci.* **1994**, *29*, 6159.
(36) Tosaka, M.; Kamijo, T.; Tsuji, M.; Kohjiya, S.; Ogawa, T.; Isoda, S.; Kobayashi, T. *Macromolecules* **2000**, *33*, 9666.
(37) Natta, G.; Corradini, P.; Bassi, I. W. *Nuovo Cimento Suppl.* **1960**, *15*, 52.
(38) Turner-Jones, A. *J. Polym. Sci., Part B: Polym. Phys.* **1963**, *1*, 455.
(39) Boor, J., Jr.; Mitchell, J. C. *J. Polym. Sci. Part A Polym. Chem.* **1963**, *1*, 59.
(40) Olley, R. H.; Hodge, A. M.; Bassett, D. C. *J. Polym. Sci., Polym. Phys.* **1979**, *17*, 627.
(41) Khoury, F.; Barnes, J. D. *J. Res. Natl. Bur. Std.* **1972**, *76A*, 225.
(42) Lotz, B.; Cheng, S. Z. D. *Polymer* **2005**, *46*, 577.
(43) Khoury, F.; Passaglia, E.; *Treatise on Solid State Chemistry*; Plenum Press: New York; 1976; Vol. 3; Chapter 6.
(44) Yamashita, M.; Kato, M. *J. Appl. Crystallogr.* **2007**, *40*, s650.
(45) Qiang, F.; Heck, B.; Strobl, G.; Thomann, Y. *Macromolecules* **2001**, *34*, 2502.
(46) Ferry, J. D.; *Viscoelastic Properties of Polymers*, 3rd ed.; Wiley: New York; 1980.
(47) Gaur, U.; Wunderlich, B. *J. Phys. Chem. Ref. Data* **1983**, *12*, 29.
(48) Keddie, J. L.; Jones, R. A. L.; Cory, R. A. *Europhys. Lett.* **1994**, *27*, 59.
(49) Forrest, J. A.; Dalnoki-Veress, K. *Adv. Colloid Interface Sci.* **2001**, *94*, 167.
(50) Alcoutlabi, M.; McKenna, G. B. *J. Phys.: Condens. Matter* **2005**, *17*, R461.
(51) McKenna, G. B. *Eur. Phys. J. Special Topics* **2007**, *141*, 291.
(52) Hobbs, J. K.; Humphris, A. D. L.; Miles, M. J. *Macromolecules* **2001**, *34*, 5508.